Simple model of energy deposition by suprathermal electrons in laser-irradiated targets

Robert J. Harrach and Ray E. Kidder
Lawrence Livermore National Laboratory, Livermore, California 94550
(Received 25 August 1980)

Energy deposition (preheat) by suprathermal electrons in laser-irradiated targets is described using a model based on Spencer's electron transport calculation. Approximate analytical, as well as numerical, solutions are found for the specific energy deposition $\mathcal{S}_{dep}(J/g)$ and fraction f of energy transmitted beyond a given depth, measured in curvilinear ranges. Example calculations are presented for homogeneous targets of gold, aluminum, and carbon. The application of the model to treat multilayer composite targets is briefly considered. The parametric dependence of these results reveal that the most significant parameter by far is the source temperature T_h of the hot or suprathermal electrons. The predictions of the preheat model are shown to be in good agreement with experimental data on gold and aluminum disks irradiated by Nd-glass laser pulses at the 10^{15} W/cm^2 level. Included in the theory-data comparison are predictions for these experiments based on several other simple models and large code simulations of the experiments. Future aluminum disk experiments in which T_h is accurately measured could provide a sensitive test for the theories.

I. INTRODUCTION

A problem of central importance in laser fusion and laser equation-of-state (EOS) studies is target preheat by suprathermal electrons generated near the critical density surface of a laser-irradiated pellet or disk. These very penetrating electrons run into the target ahead of the ablation shock wave. The energy they deposit heats the target core, degrading the implosion in the laser fusion experiment, or deleteriously perturbing the initial state in the laser EOS experiment.

This phenomenon is currently modeled in large laser-plasma-hydrodynamics computer codes using descriptions based on multigroup flux-limited diffusion theory, or Monte Carlo methods. It is desirable to have a much simpler description to gain insight into the relative importance of different physical parameters and to expedite target design for experiments, leaving more detailed but closely and time-consuming large code calculations to do fine tuning on a near-optimum design. Previous theoretical models[1,2] based on single-group steady-state diffusion theory have had some success in describing high Z materials, e.g., gold, in which electron-ion scattering is dominant. The simple diffusion theory approximation breaks down for lower atomic numbers and for targets which are thin compared to several mean free paths for electron-ion scattering.

The model we present is based on a calculation of electron transport by Spencer,[3] using his moments method. After deriving the model in Sec. II, we apply it to several specific target media in Sec. III. The expressions we obtain for energy deposition versus distance in gold, aluminum, and carbon, representing high, medium, and low atomic numbers, have a surprisingly high degree of analytical simplicity. The predicted sensitivity of electron energy deposition to various parameters—laser intensity and wavelength, target thickness, and target composition—is briefly discussed in Sec. IV. In Sec. V we show that the results of the model agree well with experimental data reported for gold[4,5] and aluminum[2] targets irradiated by Nd-glass laser pulses. Also included in the comparison are predictions for these experiments based on several other simple analytical models and numerical results derived from large computer code simulations of the experiments. The results for aluminum are shown to be especially sensitive to the value of the hot electron source temperature, T_h, suggesting the importance of future Al disk experiments in which T_h is accurately measured. In Sec. VI we remark on the application of our model to describe hot electron preheat in multilayer composite targets. Finally, a brief summary and conclusion is given in Sec. VII.

II. DERIVATION OF THE MODEL

The model we adopt is shown schematically in Fig. 1. Its main features are distilled from the following widely accepted picture of the laser-plasma interaction process. Intense laser radiation propagates through a corona of hot blow-off plasma ablated from the target. The laser beam is attenuated by inverse bremsstrahlung (IB) absorption as it propagates up the plasma density gradient. Electrons heated by the IB mechanism comprise a thermal or cool, in contrast to suprathermal or hot, Maxwellian distribution. A turning point is reached by a laser ray at a location (or before, depending on the angle of incidence of the ray) where the density of plasma-free electrons equals the critical density n_c (cm^{-3}) $\cong 10^{21}/[\lambda(\mu\text{m})]^2$, where λ is the laser wavelength.

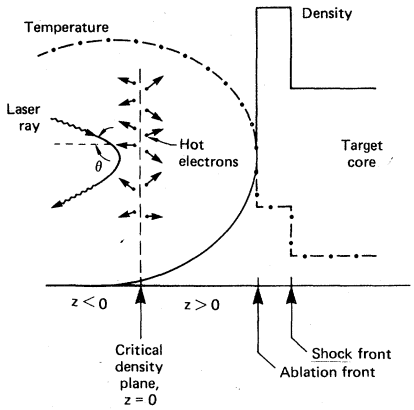

FIG. 1. Schematic diagram of the laser-plasma interaction, showing variation of target temperature and density with position. Laser light penetrates to the critical density surface or less, depending on the angle of incidence θ of a ray. The distribution of suprathermal electrons generated near the critical surface by resonance absorption of laser radiation is approximated as a plane isotropic electron source, with Maxwellian velocity distribution characterized by a temperature T_h. Hot electrons emitted or back-scattered into the half-space $z<0$ away from the target core are reflected back by space-charge electric fields, ultimately depositing their energy in the dense core along with all other hot electrons.

Of the laser energy that survives to reach the turning point, part is reflected back through the plasma; the remainder is absorbed by collective or resonant effects, going into the production of a distribution of suprathermal electrons at the critical density surface.[6] The overall fraction of laser intensity absorbed by suprathermal electrons is written as σI_0, where $I_0 = I_0(t)$ is the incident laser intensity (i.e., before interacting with the target). Hot electrons are emitted predominantly into the corona, down the plasma density gradient, but the creation of space-charge electric fields draws them back into the target core where their energy is deposited.

As indicated in Fig. 1, we assume that the critical surface plane at $z=0$ is an isotropic source of hot electrons, generated with a Maxwellian distribution of velocities corresponding to a temperature T_h (average electron energy $3kT_h/2$) which adiabatically follows the laser intensity $I_0(t)$. An approximate relation between the hot electron temperature and laser intensity, neglecting a weak dependence on the cool or thermal electron temperature and an even weaker dependence on the ion temperature, is[7]

$$kT_h \cong a_1 (I_0 \lambda^2)^{a_2} , \tag{1}$$

where I_0 is expressed in units 10^{14} W/cm^2, λ in μm, kT in keV, and a_1, a_2 are parameters with somewhat uncertain, slightly target-dependent values typically in the ranges 2 to 5 and 0.3 to 0.43, respectively. The contribution to core heating due to electrons emitted into the half-space $z<0$ (away from the core) is assumed to equal the contribution from electrons originally emitted into the core, $z>0$, due to the buildup of a repelling space-charge barrier.

The principal quantity we want to derive is the energy deposition function $W_{\rm dep}(l)$ which specifies the amount of electron energy deposited per unit cross sectional area, between concentric spherical or parallel plane surfaces at $z=0$ and $z=l$. Throughout this paper, distances such as z and l are expressed in units g/cm^2; that is, they represent an integral of the target density over length traversed by an electron. The z direction is chosen to lie perpendicular to the source plane at $z=0$ and the observation plane at $z=l$.

For its derivation it is useful to express the desired energy deposition function $W_{\rm dep}(l)$ in the form

$$W_{\rm dep}(l) = \int_{-\infty}^{\infty} dt \int_{-\infty}^{\infty} d^3v \int_0^l dz\ \dot{\mathcal{E}}_{\rm dep}(z,v) , \tag{2}$$

in which t is the time, $d^3v = dv_x\, dv_y\, dv_z$ is a three-dimensional velocity element, l is a penetration depth (mass per unit area), and $\dot{\mathcal{E}}_{\rm dep}(z,v)d^3v$ gives the specific rate of energy deposition (energy per sec per gram) in a plane of thickness dz at z due to electrons having source plane velocities in the interval $(\vec{v},\ \vec{v}+d\vec{v})$. The specific-energy deposition rate $\dot{\mathcal{E}}_{\rm dep}(z,v)$ can be expressed in terms of Spencer's[3] dimensionless energy dissipation function J for a monoenergetic electron source. The result is

$$\dot{\mathcal{E}}_{\rm dep}(z,v)d^3v\, dz = 2\dot{N}_0 \left(\frac{dE}{dr}\right)_v J_{\rm PI}(x)\hat{f}(v)d^3v\, \frac{dz}{\mathfrak{N}} . \tag{3}$$

On the right-hand side of Eq. (3), $(dE/dr)_v$ is the stopping power for electrons with initial velocity v, where E is the electron kinetic energy and r is distance in (g/cm^2) along the actual path of electron motion. $J_{\rm PI}(x)$ is a dimensionless energy dissipation function.[8] Its dimensionless argument x represents the perpendicular (z-directed) distance from the source plane $z=0$ to the parallel plane at z, normalized to the curvilinear or residual range $r_0 = r_0(v)$(g/cm^2):

$$r_0(v) = \int_0^E \frac{dr}{(dE/dr)_v} , \quad E = mv^2/2 , \tag{4}$$

$$x = /r_0(v) . \tag{5}$$

$\hat{f}(v)$ denotes the velocity distribution of electrons in the source plane, which we take to be Maxwellian:

$$\hat{f}(v)=\left(\frac{m}{2\pi kT_h}\right)^{3/2}\exp\left(-\frac{mv^2}{2kT_h}\right), \tag{6}$$

where m is the electron rest mass and k is Boltzmann's constant. $\dot{N}_0$ is the total number of electrons generated in the source plane per sec per unit area. For the laser problem, we have

$$\dot{N}_0=\frac{\sigma I_0(t)}{(3/2)kT_h}, \tag{7}$$

where $I_0(t)$(W/cm^2) is the time-dependent incident laser intensity and σ is the fraction channeled into hot electron production. The factor $\mathfrak{N}$ in Eq. (3) is a normalization constant discussed below.

The quantity $J_{PI}(x)$ in Eq. (3) is a dimensionless energy deposition function for a plane isotropic (PI) source of electrons. Since Spencer[3] evaluates J's only for plane perpendicular (PP) and point isotropic (PtI) sources, it is necessary to derive J_{PI}. It is easily found that

$$J_{PI}(x)=\int_x^\infty \frac{J_{PtI}(\mu)}{2\mu}\,d\mu . \tag{8}$$

Table I gives computed values of $J_{PI}(x)$ for carbon, aluminum, and lead, for the initial energy $E=25$ keV. An important property of the J functions is their insensitivity to electron energy E; e.g., the difference between J vs x curves for 25 and 50 keV is negligible for our purposes. However, a very significant implicit dependence of J on E enters through the E or v dependence of the argument $x=z/r_0(v)$. Another convenient property is that the J's change only slightly with Z for large Z, e.g., the J values for gold ($Z=79$) are practically the same as for lead ($Z=82$).

Integrating Eq. (3) over the distribution of electron velocities, Eq. (6), and also integrating over the full time duration of the laser pulse, we find a relation for the total energy per gram, $\mathcal{E}_{dep}(z)$, deposited in a plane of thickness dz at depth

TABLE I. Dimensionless energy dissipation function J_{PI} for a plane isotropic source of electrons with starting energy $E=25$ keV.

x	$J_{PI}(x)$ Carbon	Aluminum	Lead
0.025	2.74	3.05	5.15
0.1	2.00	2.28	3.36
0.2	1.59	1.76	1.49
0.3	1.29	1.33	0.43
0.4	1.01	0.921	0.073
0.5	0.749	0.547	5.2×10^{-3}
0.6	0.488	0.247	$\sim10^{-4}$
0.7	0.243	0.0671	
0.8	0.059	5.2×10^{-3}	
0.9	5.5×10^{-4}	4.6×10^{-6}	

z(g/cm^2):

$$\mathcal{E}_{dep}(z)dz=\int_{-\infty}^{\infty}dt\int_0^\infty 4\pi v^2dv\;\dot{\mathcal{E}}_{dep}(z,v)dz , \tag{9}$$

which gives

$$\mathcal{E}_{dep}(z)dz/W_{abs}=\mathcal{J}(x_0)dx_0\Big/\int_0^\infty \mathcal{J}(x_0')dx_0' . \tag{10}$$

Here, W_{abs} is the total laser fluence (energy per unit area) absorbed in the source plane:

$$W_{abs}=\sigma\int_{-\infty}^{\infty}I_0(t)dt , \tag{11}$$

and $\mathcal{J}(x)$ is an integral[9] over the Maxwellian velocity distribution, Eq. (6):

$$\mathcal{J}(x_0)=\int_0^\infty\left(\frac{dE}{dr}\right)_y J_{PI}(x(x_0,y))y^2e^{-y^2}dy , \tag{12}$$

where y is a dimensionless velocity variable,

$$y=v/(2kT_h/m)^{1/2} \tag{13}$$

and the normalized distance variables x and x_0 are defined by

$$x(x_0,y)=z/r_0(y)=x_0r_0(1)/r_0(y) , \tag{14}$$

$$x_0=[x]_{y=1}=z/r_0(1) . \tag{15}$$

That is, x_0 is measured in curvilinear ranges $r_0(1)\equiv r_0(kT_h)$ for electrons with initial energy kT_h or velocity $(2kT_h/m)^{1/2}$. Rewriting Eq. (2) in terms of the variable $\mathcal{E}_{dep}(z)$, we have

$$W_{dep}(l)=\int_0^l \mathcal{E}_{dep}(z)dz . \tag{16}$$

The normalization of $\dot{\mathcal{E}}_{dep}(z,v)$ has been chosen[10] to assure that conservation of energy is satisfied, i.e.,

$$W_{dep}(\infty)=\int_0^\infty \mathcal{E}_{dep}(z)dz=W_{abs} . \tag{17}$$

III. RESULTS OF THE MODEL FOR C, Al, AND Au

Application of the basic equations of our model, Eqs. (10), (12), and (16), to a specific target medium requires knowledge of $J_{PI}(x)$ and data on electron stopping power dE/dr and electron range r_0 as functions of starting energy $E=mv^2/2$. Reference 11 provides accurate data on dE/dr and r_0 for a wide range of materials.

Our procedure is to fit the numerical data for these three functions by simple analytical expressions valid throughout the electron energy range of interest (about 1 to 200 keV). Then the integrals of the model are evaluated analytically (as well as numerically) to get expressions for $\mathcal{E}_{dep}(z)$ and $W_{dep}(l)$.

Data[11] on electron stopping power and range in Au, Al, and C over the range $1 \leq E \leq 200$ keV are fairly closely approximated by expressions of the form

$$\frac{dE}{dr} = aE^{-\mu} , \tag{18}$$

$$r_0(E) = bE^{1+\mu} , \tag{19}$$

where $E = mv^2/2$ is the initial energy of the electrons and a, b, and μ are constants for a given material. Table II gives their values for C, Al, and Au, and Fig. 2 illustrates the accuracy of Eq. (19) for gold and aluminum.

Similarly, energy deposition functions $J_{PI}(x)$ for the three target materials, given earlier in Table I, are represented accurately enough for our purposes by the following analytical expressions. For gold (or lead),

$$J_{PI}(x) \cong (4.7)e^{-27x^2}, \quad 0 \leq x \leq \infty \tag{20}$$

and for aluminum and carbon,

$$J_{PI}(x) \cong \begin{cases} A(1 - Bx), & 0 \leq x \leq B^{-1} \\ 0, & x > B^{-1} , \end{cases} \tag{21}$$

with[12] $A = 2.75$, $B = 1.6$ for Al and $A = 2.2$, $B = 1.25$ for C.

Substituting the approximate analytical relations given by Eqs. (18), (19), and (20) or (21) into Eq. (12), we find that the integral $\mathcal{J}(x_0)$ takes the form

$$\mathcal{J}(x_0) = \frac{C_1}{(kT_h)^{\mu}} Y(x_0) , \tag{22}$$

where kT_h is measured in keV, C_1 is a constant [with units $(\text{keV})^{1+\mu}/(\text{g/cm}^2)$, for example] and Y is an integral over the source velocities which depends on the dimensionless depth x_0. $\mathcal{J}(x_0)$ is measured in units of keV/g/cm^2. In particular, for gold, aluminum, and carbon, respectively:

$$\mathcal{J}(x_0) = \begin{cases} \dfrac{1.6\times10^5}{(kT_h)^{0.6}} \displaystyle\int_0^{\infty} y^{0.8} \exp\left(-y^2 - \frac{27x_0^2}{y^{6.4}}\right) dy & \text{(23a)} \\ \dfrac{2.34\times10^5}{(kT_h)^{0.72}} \displaystyle\int_{\nu(x_0)}^{\infty} y^{0.56}\left[1 - \left(\frac{\nu(x_0)}{y}\right)^{3.44}\right] e^{-y^2} dy & \text{(23b)} \\ \dfrac{2.86\times10^5}{(kT_h)^{0.78}} \displaystyle\int_{\nu(x_0)}^{\infty} y^{0.44}\left[1 - \left(\frac{\nu(x_0)}{y}\right)^{3.56}\right] e^{-y^2} dy , & \text{(23c)} \end{cases}$$

where, in Eq. (23b) for aluminum the function $\nu(x_0)$ is given by $\nu(x_0) = (1.6x_0)^{1/3.44}$ and in Eq. (23c) for carbon it is $\nu(x_0) = (x_0/0.8)^{1/3.56}$. The parameter x_0 is given, as before, by

$$x_0 = z/r_0(kT_h) ,$$

and the relationship between x_0, x, and the velocity- (y-) dependent curvilinear range $r_0(y)$ is

$$x = z/r_0(y) = x_0 y^{-2(1+\mu)} , \tag{24}$$

since, from Eqs. (13) and (19),

$$r_0(y) = r_0(kT_h) y^{2(1+\mu)} . \tag{25}$$

Numerical integration of the y integrals in Eqs. (23a)–(23c) produces the curves for $\mathcal{J}$ vs x_0 shown in Fig. 3. A second numerical integration

TABLE II. Parameters a, b, and μ in the stopping power and range-energy relations, Eqs. (18) and (19), for carbon, aluminum, and gold, based on Ref. 11.

Material	a $[(\text{keV})^{1+\mu}/(\text{g/cm}^2)]$	b $[(\text{g/cm}^2)/(\text{keV})^{1+\mu}]$	μ
C	1.3×10^5	4.6×10^{-6}	0.78
Al	8.5×10^4	6.77×10^{-6}	0.72
Au	3.4×10^4	1.9×10^{-5}	0.6

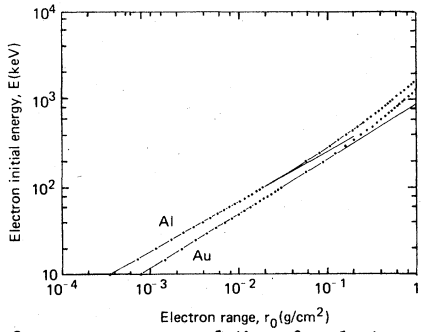

FIG. 2. Range-energy relations for electrons in aluminum and gold from Ref. 11. r_0 is the curvilinear or residual range measured along the path of motion. The straight lines, corresponding to Eq. (19) with parameters as given in Table II, are suitable approximations below about 200 keV.

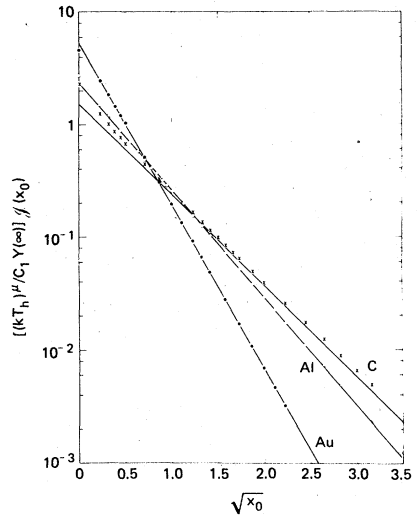

FIG. 3. Variation of the integral $\mathcal{J}(x_0)$ vs $\sqrt{x_0}$, for carbon, aluminum, and gold targets. The points are derived from numerical integrations of Eqs. (23a)–(23c); the straight lines are given by the equation

$$\frac{(kT_h)^\mu}{C_1 Y(\infty)}\,\mathcal{J}(x_0) = \alpha e^{-\beta\sqrt{x_0}}\,,$$

with values of parameters from Table III.

to evaluate $\int \mathcal{J}\,dx_0$ gives the desired final results for the energy deposition shown by the points in Fig. 4. Specifically, Fig. 4 shows the fraction f of hot electron energy transmitted beyond a depth $x_0(l)$, where

$$f \equiv 1 - [W_{\rm dep}(l)/W_{\rm abs}]\,, \tag{26}$$

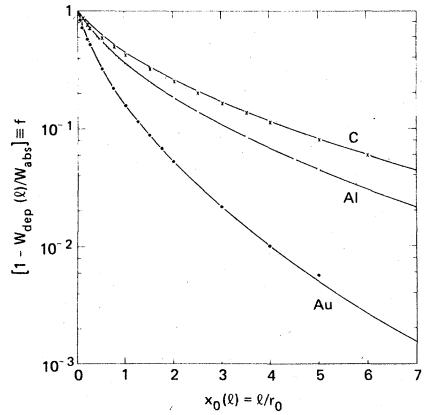

FIG. 4. Fraction f of electron energy transmitted beyond dimensionless depth $x_0(l)$ in carbon, aluminum, and gold. The points are obtained by numerically intergrating the equations of the preheat model; the solid curves follow the analytical approximation, Eq. (31).

$$\frac{W_{\rm dep}(l)}{W_{\rm abs}} = \frac{\int_0^l \mathcal{E}_{\rm dep}(z)\,dz}{W_{\rm abs}} = \frac{\int_0^{x_0(l)} \mathcal{J}(x_0)\,dx_0}{\int_0^\infty \mathcal{J}(x_0)\,dx_0}\,, \tag{27}$$

and

$$x_0(l) = l/r_0(kT_h)\,. \tag{28}$$

Though the equations of our model are not complicated and their numerical solution is easily carried out on a pocket programmable calculator, the appeal of the model is greatly enhanced by expressing the solutions in analytical form. We find that all three of the curves in Fig. 3 are closely approximated by the functional form $\mathcal{J}(x_0) \propto \exp(-\beta\sqrt{x_0})$, or

$$\mathcal{J}(x_0)\Big/\int_0^\infty \mathcal{J}(x_0)\,dx_0 = \frac{\beta^2 e^{-\beta\sqrt{x_0}}}{2}\,, \tag{29}$$

with values of the material-dependent constants as given in Table III. Thus the specific energy deposition is given by

$$\mathcal{E}_{\rm dep}(l) = [\,W_{\rm abs}/r_0(kT_h)]\,\frac{\beta^2}{2}\exp(-\beta\sqrt{x_0(l)})\,. \tag{30}$$

The great utility of Eq. (29) or (30) is its easy integrability, yielding analytical expressions for the total transmitted and deposited energy:

$$\begin{aligned} f(l) &= (1+\beta\sqrt{x_0(l)})e^{-\beta\sqrt{x_0(l)}} \\ &= 1 - W_{\rm dep}(l)/W_{\rm abs}\,. \end{aligned} \tag{31}$$

As indicated in Fig. 4, this equation agrees with the corresponding numerical results of our model to within 5% in all three materials for f values down to 10^{-2}, and the error increases slowly for greater levels of attenuation.

Equations (30) and (31) comprise the major accomplishment of our simple model of preheat by suprathermal electrons. These expressions imply that the electron energy deposition in these three quite dissimilar materials Au, Al, and C (and presumably others), is represented to a good approximation by a single "universal" curve, shown in Fig. 5.

TABLE III. Parameters appearing in the exponential approximation to $\mathcal{J}(x_0)$ for gold, aluminum, and carbon:

$$\frac{\mathcal{J}(x_0)}{\{Y(\infty)C_1/[kT_h(\text{keV})]^\mu\}} \cong \alpha\exp(-\beta\sqrt{x_0})$$

Material	α	β	$Y(\infty)$	$C_1\frac{(\text{keV})^{1+\mu}}{(\text{g/cm}^2)}$	μ
Au	5.35	3.31	0.118	1.6×10^5	0.6
Al	2.30	2.17	0.213	2.34×10^5	0.72
C	1.5	1.85	0.272	2.86×10^5	0.78

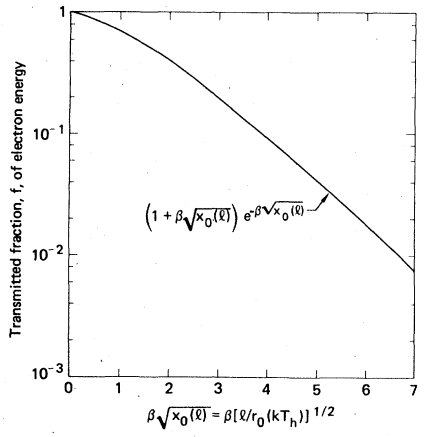

FIG. 5. Universal curve [Eq. (31)] describing the fraction of suprathermal electron energy transmitted beyond a depth l (g/cm^2) for arbitrary electron source temperature T_h and target material parameters β, r_0.

IV. PARAMETRIC DEPENDENCES

The model's predictions regarding sensitivity of electron energy deposition to different parameters is readily seen using Eq. (31). Laser and target properties enter only through the product of factors $\beta[x_0(l)]^{1/2}=\beta[l/r_0(kT_h)]^{1/2}$. As noted earlier the electron range function $r_0(E)$ is tabulated for many materials and follows the power law given in Eq. (19) over the limited energy region of interest. The characteristic energy value $E=kT_h$ depends on laser intensity and wavelength approximately as in Eq. (1). The parameter β varies for different target materials as indicated in Table III for Au, Al, and C. Interpolating between these three data points, we see in Fig. 6 that the value of β for a material of arbitrary Z should be given roughly by

$$\beta \cong (0.59)\ln(Z/0.3)\ . \tag{32}$$

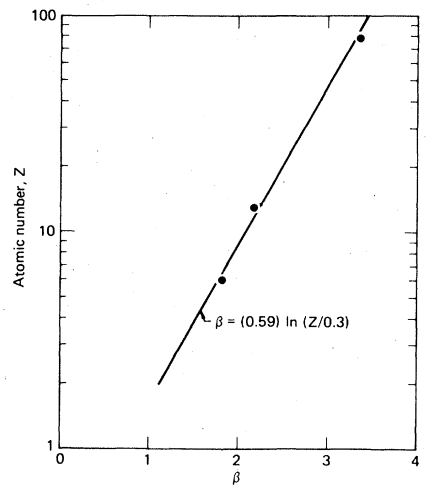

FIG. 6. Variation of parameter β with atomic number Z.

Combining these results, we have

$$\beta\sqrt{x_0(l)} \cong \frac{(0.59)\ln(Z/0.3)\sqrt{l/b}}{(kT_h)^{(1+\mu)/2}}\ , \tag{33}$$

where the constants μ and b from Eq. (19) are identified using range-energy data, as in Table II, and kT_h is evaluated, e.g., using Eq. (1). By far the dominant sensitivity is to the hot electron temperature, with a concomitant strong dependence of hot electron preheat on laser wavelength and intensity. Specific examples are treated in the following section.

V. COMPARISON TO EXPERIMENTAL RESULTS AND OTHER CALCULATIONS

Data on suprathermal electron energy deposition has recently been reported for Nd-glass-laser irradiation experiments on gold[4,5] and aluminum[2,13] disks at the 10^{15} W/cm^2 intensity level. In this section we compare this data with the predictions of our model, other simple models, and large-code numerical simulations.

In both sets of experiments the principal diagnostic for inferring hot electron energy deposition (preheat) is a determination of the temperature history of the back surface of the disk by measuring rear surface luminosity versus time using an optical streak camera. The theory-experiment comparison therefore necessitates an equation-of-state model to determine the temperature rise associated with a given amount of preheat. We adopt a simple analytical EOS model for multiply ionized matter due to Zeldovich and Raizer[14,15] to describe gold and aluminum plasmas in the 10^{-1} to 10^2 eV temperature range. We find that between about 2 and 100 eV the EOS model results are fairly well represented by the following formulas. For gold, the specific internal energy as a function of temperature and density is given by

$$\mathcal{E} \cong (kT)^{1.9} q_{\mathrm{Au}}(\rho_0)\ , \tag{34}$$

where $\mathcal{E}$ is measured in kJ/g, kT in Ev, and the density-dependent coefficient q_{Au} equals 1.4, 0.8, and 0.5 for $\rho_0=10^{-2}$, 10^{-1}, and 1 g/cm^3, respectively. Similarly for aluminum in this temperature range,

$$\mathcal{E} \cong (kT)^{1.55} q_{\mathrm{Al}}(\rho_0)\ , \tag{35}$$

with $q_{\mathrm{Al}} \cong 12.6$, 8.7, and 5.3 for $\rho_0=10^{-2}$, 10^{-1}, and 1 g/cm^3, respectively. In the temperature range below 2 eV, this EOS model predicts that

the internal energy asymptotically approaches a density-independent value given by $\mathcal{E}(\mathrm{kJ/g}) \cong (0.734)kT$ (eV) for gold, and $\mathcal{E}(\mathrm{kJ/g}) \cong (5.37)kT \times (\mathrm{eV})$ for aluminum.

The gold disk experiments of Rosen *et al.*[4,5] featured 2 to 25-μm-thick disks that were irradiated over a spot size roughly 180 μm in diameter using 800 J of Nd-glass (1.06-μm) laser light in a pulse of about 1-ns duration and nominal peak intensity 3×10^{15} W/cm^2. Since the spot size is large compared to the thickness, the hot electron preheating should be one dimensional to a good approximation. Rosen *et al.* inferred from x-ray measurements that 4 J out of the 800 J incident went into hot electrons; thus the absorption parameter σ is estimated to be $4/800 = 0.005$. They also concluded from the observed x-ray emission spectrum that the peak value of the hot electron temperature was $kT_h \cong 35$ keV.

A comparison of data and calculations for the gold disk experiments is shown in Table IV. Results derived using the models of Caporaso and Wilson,[1] Lee and Trainor,[2] Rosen,[16] and the present authors are shown along with those from Rosen's detailed numerical simulations.[16] As mentioned previously, the models of Refs. 1 and 2 are based on steady state diffusion theory. Rosen's model consists simply of a postulated form for the differential equation governing the decline of electron energy with distance into the target. The theoretical predictions are compared both with regard to temperature and specific energy deposition at the back of the target, but only the temperature was measured in the experiments.

The necessity of going through an EOS calculation to derive a temperature, before comparison can be made with the data, dims the discrimination between various theoretical models of hot electron preheat. Inaccuracies associated with a given EOS then come into play, and part of the discrepancy between calculated temperatures in Table IV originates from the use of different EOS models. Furthermore a substantial uncertainty is associated with what density to use for the back surface layer, since this state variable was not measured. In most of the laser shots a kilojoule or more per gram was deposited in this layer, which is easily enough to vaporize the material, producing densities of about 10^{-1} to 10^{-2} g/cm^3. For thicker targets and/or lower laser intensities a value of ρ_0 closer to normal density is more appropriate.

Inspecting Table IV with these reservations in mind, we conclude that all of the calculations are in reasonably close qualitative and quantitative agreement, both with respect to each other and the experimental data on the scale of accuracy

TABLE IV. Comparison of data and calculations for gold disks irradiated by Nd-glass laser pulses (ln s duration, 3×10^{15} W/cm^2 intensity, 1.06-μ, wavelength).

Gold disk thickness, (l/ρ_0) (μm)	Predicted total energy per gram deposited at rear of target by hot electrons $\mathcal{E}_{\mathrm{dep}}$ (kJ/g)						Back surface temperature rise, kT (eV)				
	Present model[a]	CW model[a] (Ref. 1)	LT model[a] (Ref. 2)	Rosen model[a] (Ref. 16)	Simulation[b] (Ref. 16)	Expt. (Refs. 4, 5)	Present model[c]	CW model[c] (Ref. 1)	LT model[d] (Ref. 2)	Rosen model[d] (Ref. 16)	Simulation[b] (Ref. 16)
2	946	540	430	1000	4000	8 to 32	31.5	24	22	35	25–35
14.5	10.3	3.4	4.07	3	1	$\leqslant 1$	2.6	1.6	1.4	0.5	0.1–0.3
25	1.08	0.36	0.524	0.05	$\leqslant 10^{-8}$	$\leqslant 1$	0.89	0.4	$\leqslant 1$	0.01	<0.1

[a] Values computed using $\sigma = 0.005$, $kT_h = 35$ keV, $\tau_L \cong 1$ nsec, $I_{0,\max} = 3\times10^{15}$ W/cm^2.
[b] Simulations by M. Rosen (Ref. 16) using the LASNEX code.
[c] Values calculated assuming the density at the back surface of the disk to be $\rho_0 = 0.01$ g/cm^3.
[d] Values calculated assuming the density at the back surface of the disk to be $\rho_0 = 0.1$ g/cm^3.

set by the experimental measurements. Generally, Rosen's simulations using the laser-plasma-hydrodynamics code LASNEX[17] predict a more severe attenuation of hot electron transport in gold than is indicated by the models. The models give an exponential decline of $\mathcal{E}_{dep}$ with distance, going as $\exp[-b_1 x_0(l)^{b_2}]$, where b_1 and b_2 are constants with $b_2 = 1$, $\frac{1}{2}$, $\frac{2}{5}$, and $\frac{1}{3}$ for the models of Rosen,[16] ourselves, Caporaso and Wilson,[1] and Lee and Trainor,[2] respectively. Apart from such differences in detail, it appears that all of the calculations properly account for the important gross features of the data, e.g., that prompt preheat by hot electrons is very substantial for the 2-μm gold disk but practically negligible at 25 μm.

In the aluminum disk experiments of Trainor and Holmes[2,13] the disk thickness and laser pulse duration were kept fixed at 12.5 μm and 0.3 ns, respectively. Data were taken at two levels of intensity separated by a factor of about two. The parameter σ was estimated to be 0.3, based on earlier similar experiments. The hot electron temperature at the critical density surface was assumed to be given by Eq. (1) with suitable values chosen for the parameters a_1 and a_2, about which we will say more.

Table V presents the data and compares the predictions of our model with ones reported by Lee and Trainor[2] for these measurements. A couple of extra intensity values are added to better compare the calculations.

We find for these aluminum disk irradiations that the calculated energy deposition is extremely sensitive to the values we select for the poorly known parameters a_1 and a_2 in the formula for T_h. The reason is that the exponent $\beta\sqrt{x_0(l)}$ in Eq. (30), involving the dimensionless penetration depth $x_0(l) = l/r_0(kT_h)$, has quite large and intensity-sensitive values for the 12.5-μm-thick aluminum disk. As Eq. (33) shows, this is principally due to the smallness of the curvilinear range r_0 and its strong dependence on hot electron temperature: $r_0(kT_h) \cong 6.77\times10^{-6}\ (kT_h)^{1.72}$. For example, let the exponent a_2 in Eq. (1) have the often quoted value $a_2 = 0.425$, and examine the effect on $\mathcal{E}_{dep}$ of several different but reasonable choices for a_1, e.g., $a_1 = 2.6$, 3.54, and 5.2. Then for the 5.1×10^{14} W/cm^2 intensity we calculate that the specific energy deposited in the back surface layer (assuming $\sigma = 0.3$) is, respectively, 11.2, 90.4, or 530 (kJ/g). We find that our energy deposition model and EOS model give full agreement with the measured back surface temperatures if, for aluminum, the choices $a_1 = 3.54$, $a_2 = 0.425$ are used in Eq. (1). Lee and Trainor used the same a_2 but set $a_1 = 2.6$. We conclude that an accurate independent determination of T_h in the aluminum experiments, as was strived for in the gold experiments, would provide a critical test of different theoretical models.

VI. MULTILAYER TARGETS

Up to this point we have assumed the target is a single homogeneous medium, but our model can be used to estimate hot electron preheat in the important practical case of a multilayer composite target. To illustrate the procedure, we consider the simple example of a two-layer disk composed of a fairly transparent (to hot electrons) material A backed by a strongly scattering material B in which we want to evaluate hot electron preheat. The semi-transparency of the front disk may be due to its thinness or low atomic number or both. The idea is to replace the A layer by an equivalent thickness of B material so

TABLE V. Comparison of data and calculations for 12.5-μm thick aluminum disks irradiated by Nd-glass laser pulses (0.3 ns duration, 1.06-μm wavelength).

Laser intensity, $I_{0,max}$ (10^{14} W/cm^2)	Assumed hot electron temperature, kT_h(keV)		Predicted total energy deposited per gram at rear of target by hot electrons, $\mathcal{E}_{dep}$(kJ/g)		Back surface temperature rise, kT(eV)			
	Present model	LT model (Ref. 2)	Present model[a]	LT model[a] (Ref. 2)	Expt.[b]	Present model[c]	LT model[c] (Ref. 2)	Simulation[d]
1.0	3.72	2.73	0.052	0.295		0.04	<0.1	
2.0	4.99	3.67	2.08	5.03		0.40	0.5	
2.7	5.69	4.17	8.22	15.	1.0	0.96	1.2	2.5
5.1	7.43	5.46	90.4	120.	4 to 5	4.53	4.1	

[a] Values computed using $\sigma = 0.3$, $\tau_L = 0.3$ ns, $l = 3.375\times10^{-3}$ g/cm^2 and I_{0max}, kT_h as indicated.
[b] Data obtained by J. Trainer and N. Holmes (Ref. 13).
[c] Values calculated assuming the density at the back surface to be $\rho_0 = 0.1$ g/cm^3.
[d] Simulation by Y. Lee (Ref. 2) using the LASNEX code.

that we can deal with a target composed entirely of B material.

The equivalence is defined in terms of the energy transmission factor $f(l)$ [Eq. (3.1)]. The thickness l_A(g/cm^2) of material A is to be replaced by a thickness $l_B^{\rm eff}$ of B such that hot electron energy transmission through the two are equal, taking into account the copious backscattering of electrons into A from B. The original composite A-B target of thickness $(l_A + l_B)$ is thus replaced by a homogeneous $B^{\rm eff} - B$ one of thickness $(l_B^{\rm eff} + l_B)$. This procedure can be generalized to an arbitrary number of layers of any materials A, B, C, ..., first forming $B^{\rm eff} - B$ from $A - B$, then $C^{\rm eff} - C$ from $(B^{\rm eff} - B) - C$, etc., taking into account at each step the difference in albedoes or effective electron energy reflection coefficients of the adjacent layers.

A relation for the energy transmission factor $f_A(x_A)$ for hot electrons through material A to the $A - B$ interface at depth x_A is

$$f_A(x_A) \cong \frac{(1-\mathcal{R}_B) f_A^{(0)}(x_A)}{[1-\mathcal{R}_B f_A^{(0)}(2x_A)]} . \tag{36}$$

Here the reflection coefficient or albedo $\mathcal{R}_B$ represents the effect of electron backscattering by the high-Z material B, neglecting the albedo of the semi-transparent A layer. $f_A^{(0)}$ represents the energy transmission factor for a homogeneous target [the same quantity as in Eq. (31)]. In the numerator of Eq. (36), $f_A^{(0)}$ is evaluated at the dimensionless thickness $x_A = l_A / r_0^{(A)}(kT_h)$ of the A layer; in the denominator it is evaluated at $2x_A$. The hot-electron temperature T_h is entirely determined by the A material. The derivation of Eq. (36) assumes that all the hot electrons created at the surface $x = 0$ of material A travel through A. (We assume that electrons initially directed into the region $x < 0$ of vacuum and blow-off plasma are turned back by a plasma sheath, as discussed earlier.) Some electron energy is then deposited in medium A on the electrons first transit to the $A - B$ interface. Backscattering from medium B sends back into A a fraction $\mathcal{R}_B$ of the electron energy that reaches this interface. Some of the backscattered electrons are transmitted through A, reflected by the plasma sheath, and make a second transit to the $A - B$ interface. Summing over an infinite number of such transmissions and reflections gives Eq. (36).

The defining relation for $l_B^{\rm eff}$ is obtained by equating the transmission factor $f_A(x_A)$ to one for a material B of thickness $x_B^{\rm eff} = l_B^{\rm eff} / r_0^{(B)}(kT_h)$:

$$f_B^{(0)}(x_B^{\rm eff}) = f_A(x_A) . \tag{37}$$

Inserting for $f_A^{(0)}$ and $f_B^{(0)}$ the simple forms in Eq. (31) gives an implicit equation for $x_B^{\rm eff}$:

$$(1+\xi_B^{\rm eff}) e^{-\xi_B^{\rm eff}} = \frac{(1-\mathcal{R}_B)(1+\xi_A) e^{-\xi_A}}{[1-\mathcal{R}_B(1+\sqrt{2}\,\xi_A e^{-\sqrt{2}\,\xi_A})]} , \tag{38}$$

where

$$\xi_A \equiv \beta_A [x_A(l_A)]^{1/2} , \tag{39a}$$

$$\xi_B^{\rm eff} \equiv \beta_B [x_B^{\rm eff}(l_B^{\rm eff})]^{1/2} . \tag{39b}$$

As a specific example, let material A be a 2-μm-thick layer of aluminum and B be a gold layer 10-μm thick. Further suppose that the Al front surface is irradiated by a step-function Nd-glass laser pulse with intensity 8.4×10^{14} W/cm^2, which gives $kT_h \cong 9.2$ keV. The albedo of gold can be approximated by the value[18] appropriate to a gold-vacuum interface and plane isotropic electron source distribution: $\mathcal{R}_{\rm Au} \cong 0.6$. We then find that $l_{\rm Au}^{\rm eff} \cong 10^{-3}$ (g/cm^2), or $l_{\rm Au}^{\rm eff}/\rho_0^{\rm (Au)} \cong 0.5$ μm; i.e., $\frac{1}{2}$ μm of gold is equivalent to 2 μm of aluminum in the sense of Eq. (37) at this T_h level. The description of electron energy deposition in the gold portion of the Al-Au disk then proceeds as if it were a single-layer gold disk.

VII. SUMMARY AND CONCLUSIONS

The model of hot electron preheat developed here is recommended by four principal features: a sound theoretical basis, versatility, analytical simplicity, and reasonably good agreement with experimental results obtained to date. Being based on Spencer's[3] electron transport calculation, it is applicable to materials of any atomic number, not requiring validity of a diffusion approximation. Though Spencer's theory pertains to a homogeneous medium, we have shown how the preheat model can be used to estimate energy deposition in multilayer composite targets. On the other hand, collective effects due to mutual interactions of source electrons are not included in Spencer's treatment, and therefore are missing in our model as well.

All of the important physical quantities appearing in the model, including the electron energy deposition functions $\mathcal{E}_{\rm dep}$(J/g) and $W_{\rm dep}$(J/cm^2), are expressed in terms of simple analytical formulas, making it easy to discern the various parametric dependences. The most important parameter by far is found to be the hot electron temperature, T_h, which itself depends on laser intensity and wavelength in a somewhat uncertain way. The comparisons we have presented among different

theoretical model results and experimental data suggest that future experiments, especially ones on aluminum targets in which T_h as well as the back-surface temperature is accurately measured, can provide a sensitive test for the preheat models.

ACKNOWLEDGMENT

This work was performed under the auspices of the U. S. Department of Energy by the Lawrence Livermore National Laboratory under Contract No. W-7405-ENG-48.

[1]G. J. Caporaso and S. S. Wilson, Lawrence Livermore National Laboratory Report No. UCRL-83308, 1979 (unpublished).

[2]Y. T. Lee and R. J. Trainor, Lawrence Livermore National Laboratory Report No.UCID-18574-79-4, 1980, pp. 34–41 (unpublished).

[3]L. V. Spencer, National Bureau of Standards Monograph 1, 1959 (unpublished).

[4]M. D. Rosen, Lawrence Livermore National Laboratory Report No. UCRL-83022, 1979 (unpublished).

[5]M. D. Rosen, D. W. Phillion, V. C. Rupert, W. C. Mead, W. L. Kruer, J. J. Thomson, H. N. Kornblum, V. W. Slivinsky, G. J. Caporaso, M. J. Boyle, and K. G. Tirsell, Phys. Fluids 22, 2020 (1979).

[6]J. S. Pearlman and M. K. Matzen, Phys. Rev. Lett. 39, 140 (1977); K. G. Estabrook, E. J. Valeo, and W. L. Kruer, Phys. Fluids 18, 1151 (1975); D. W. Forslund, J. M. Kindel, K. Lee, E. L. Lindstrom, and R. L. Morse, Phys. Rev. A 11, 679 (1975).

[7]K. G. Estabrook and W. L. Kruer, Phys. Rev. Lett. 40, 42 (1978).

[8]The product $(dE/dr)_v J(x)$ gives, for a point isotropic source, the energy deposited in a spherical shell of thickness $d\rho$ at radius ρ per source electron (each with initial energy $E = mv^2/2$), where $x = \rho/r_0(v)$ with $r_0(v)$ defined by Eq. (4). For a plane isotropic or plane perpendicular source this product specifies the energy dissipated per unit area in a plane layer between z and $z + dz$ by electrons having kinetic energy E at $z = 0$, normalized to one electron per unit area in the source plane.

[9]Notice that the dependence of $\mathcal{J}(x_0)$ on normalized penetration depth $x = x(y)$ enters only through the argument of J_{PI}; in the energy range of interest $x(y)$ takes the form $x = x_0 y^{-n}$, n = constant.

[10]The appropriate choice for the normalization factor $\mathfrak{N}$ in Eq. (3) is

$$\mathfrak{N} = \frac{16}{3\sqrt{\pi}} \frac{r_0(kT_h)}{kT_h} \int_0^\infty \mathcal{J}(x_0)dx_0,$$

with $\mathcal{J}(x_0)$ given by Eq. (12).

[11]M. J. Berger and S. M. Seltzer, National Aeronautics and Space Administration Report No. NASA SP-3012, 1964 (unpublished). This stopping power data pertains to cold matter, not warm plasmas, but we expect the differences would have small effect on our results.

[12]The coefficients in Eqs. (20) and (21) are chosen to give both a good fit to the numerical data and to satisfy Spencer's (Ref. 3) relation

$$\int_{-\infty}^{\infty} J_{\mathrm{PI}}(x)dx = \left(\frac{E}{r}\right) \Big/ \left(\frac{dE}{dr}\right).$$

By Eqs. (18) and (19) this approximately equals $(1 + \mu)$.

[13]R. J. Trainor and N. C. Holmes, Lawrence Livermore National Laboratory Report No. UCRL-50028-79-3, 1979, pp. 10–14 (unpublished).

[14]Y. B. Zel'dovich and Y. P. Raizer, *Physics of Shock Waves and High-Temperature Hydrodynamic Phenomena* (Academic, New York, 1966), Vol. 1, Chap. 3.

[15]Zel'dovich and Raizer's EOS model requires a knowledge of the ionization potential $I(m)$ for any degree m of ionization. For gold we use values derived from a relativistic Hartree-Fock-Slater calculation by J. H. Scofield (private communication). Those for aluminum are taken from the *Handbook of Chemistry and Physics*, edited by R. C. Weast (Chemical Rubber Co., Cleveland, 1970), 51st edition.

[16]M. D. Rosen, private communication. A description of his model will appear in Lawrence Livermore Laboratory Report No. UCRL-50021-79, 1980 (unpublished).

[17]G. B. Zimmerman and W. L. Kruer, Comments Plasma Phys. Controlled Fusion 2, 51 (1975).

[18]G. J. Lockwood, G. H. Miller, and J. A. Halbleib, IEEE Trans. Nucl. Sci. NS-22, 2537 (1975).